PCCP

PAPER

View Article Online
View Journal | View Issue

Cite this: *Phys. Chem. Chem. Phys.*, 2017, **19**, 5077

The role of OH^- in the formation of highly selective gold nanowires at extreme pH: multi-fold enhancement in the rate of the catalytic reduction reaction by gold nanowires

Riham El Kurdi and Digambara Patra*

Received 17th December 2016,
Accepted 16th January 2017

DOI: 10.1039/c6cp08607a

rsc.li/pccp

There is a quest to understand the mechanism governing the morphology and geometry control of the particle growth of nanomaterials for their optical and catalytic applications. In the available literature, the role of OH^- in dictating the size and shape of Au nanowires is unknown. As one of the first examples, herein, we explore how excess OH^- ions in CTAB micelles play a significant role during the highly selective formation of gold nanowires having controlled diameters of ~20–25 nm and length >1 μm, by reducing Au^{3+} to Au^0 in a one pot, simple synthesis procedure in the presence of Ag^+ ions. At pH 4–11, the same procedure does not harvest Au NWs, but Au NPs of diameter 50–70 nm, indicating that excess OH^- is needed for nanowire formation. XRD, TGA, DSC, EDX, FT-IR and fluorescence spectroscopic analysis confirm that both CTAB and curcumin act as capping and stabilizing agents for Au NWs as well as Au NPs – there is no remarkable difference in the curcumin/CTAB content between Au NWs and NPs prepared in different pH environments. However, changing the CTAB micellar media to DPPC liposome media inhibits the formation of nanowires at pH ~13; the growth of the Au NPs diminishes in DPPC liposomes, offering smaller NPs of diameter ~25 to 30 nm, suggesting that the role of CTAB is necessary in nanowire formation. The rate of NW formation has been found to be 0.13 h^{-1} and the growth mechanism advocates elongation in the [110] facet of Au [110] as opposed to the [100] or [111] facets. Curcumin capped Au nanowires serve as excellent nano-catalysts for the reduction of nitro-compounds and the rate of reduction of 4-nitrophenol, a model compound, by curcumin capped Au NWs is found to be ~10 fold higher, compared to Au NPs, which signifies that catalytic activities can be dictated by the size and shape of Au NPs.

Introduction

Nanostructured materials have drawn much interdisciplinary attention, since both chemical and physical properties have been found to be enhanced and can be quite fascinating in this nano-sized range.[1] Nanoparticles show properties that are often different from those of their corresponding bulk materials. Metal nanoparticles, ranging from noble to transition elements, have shown interesting properties in catalysis, optics, magnetism and sensors.[2–7] In the past few decades, gold colloids have been the subject of great interest. They are the subject of one of the most ancient themes of investigation in science; their renaissance now leads to an exponentially increasing number of publications, especially in the context of emerging nanoscience and nanotechnology, with nanoparticles and self-assembled monolayers.[8] In fact, gold nanoparticles (Au NPs) can find applications in diverse fields like medical diagnosis, catalysis, drug delivery, biosensors, cancer treatment, *etc.*;[9–12] therefore, their applications require synthesis protocols that deliver well-defined shapes and sizes.[13] Gold nanoparticles can be synthesized in different shapes, and some gold nanorods can be formed using photochemical synthesis, others can be prepared using seed-mediated growth methods.[2,14,15] The synthesis of high aspect ratio gold nano-rods has been performed *via* the wet chemical synthesis of relatively monodisperse gold.[16] In the literature, many groups have reported methods for the preparation of 1D and 2D gold nanostructures under very mild conditions.

Gold nanowires and nanosheets have been prepared *via* UV irradiation photoreduction and thermal reduction of a gold salt, $HAuCl_4$, at 70 °C in the bulk phase of poly(ethyleneoxide)–poly(propylene oxide).[17] Indeed, metal nanowires are indispensable components for the realization of nanoelectronics, and exhibit highly tunable optical properties that make them attractive candidates for several applications.[18] Nanorods and nanowires have recently been getting more attention because of

Department of Chemistry, American University of Beirut, Beirut, Lebanon. E-mail: dp03@aub.edu.lb; Fax: +9611365217; Tel: +9611350 000 ext. 3985

their anisotropic nature, although other different shapes including plates, cubes, polyhedral and breached particles of Au are also being studied.[19,20] Many studies have focused on the development of methods for the controlled synthesis of different shaped Au particles, which include photochemical, and controlled chemical reduction, microwave assisted heating, laser ablation, annealing from high-temperature solutions, metal evaporation, and sonochemical reduction.[8,21–23] The most common chemical route is precipitation of the Au NPs in aqueous solution from a dissolved gold precursor; for example $HAuCl_4$, by a reducing agent such as sodium citrate, sodium borohydride, or block copolymers.[24] The Turkevich method is the oldest and most widely employed protocol for the production of colloidal gold. It has been reported that the size can be controlled by varying the amount of sodium citrate and controlling the temperature.[13,25,26] Many groups have reported that these procedures are not environmentally friendly and as a consequence, Au NPs made by employing green chemistry principles using extracts or compounds from plants, microbes or algae are receiving considerable attention. There are rapid and convenient methods to reductively prepare gold nanoparticles from auric chloride using aqueous extracts.[27–30] Curcumin, derived from the rhizome of turmeric, is one of the cash crops extensively grown in Asia and has been used as a food spice and to treat various illnesses since ancient times.[9] Curcumin is non-toxic and environmental friendly and has been shown to exhibit antioxidant, anti-inflammatory, antimicrobial, and anticarcinogenic activities.[31,32] It is used to formulate multifunctional Au NPs that are stabilized with water soluble curcumin to target the site of action and despite a number of studies on using functionalized Au NPs for drug delivery applications, reports on the synthesis and stabilization of Au NPs using anticancer drug conjugates are scanty.[33,34] In aqueous media, cetyltrimethylammonium bromide (CTAB) has been one of the most popular molecules in the synthesis of metals, although so far, it has been limited to only gold and silver metals. Most of the synthesis methods have been performed using seed mediated growth solution with CTAB.[1,2,15,35]

Prominent work has been done, as demonstrated above, on gold nanorods, but there are very limited reports on size controlled gold nanowires (Au NWs). There is a lack of fundamental understanding of how the kinetic, thermodynamic, or other factors influence the underlying mechanism in these metal nanowires and other interesting systems.[30–33] Thus, considerable research is needed to explore the mechanisms governing the morphology and geometry control of particle growth, as they are still not well understood. The present work could serve the purpose of gaining a better understanding on how different parameters affect the formation of gold nanowires and their potential application in catalysis of the reduction of nitro-aromatics, since the reduction of organic compounds like 4-nitrophenol has been used for the detection of different proteins; however, this catalytic reduction is only limited to several colored substances, including methyl orange, 4-nitrophenol and methylene blue.[36–40] In our earlier work,[20] we reported that curcumin could help in the formation of Au nanorods through pre-reduction and it enhances Au nanorod formation prepared from CTAB capped over citrate capped Au seeds. In the available literature, the role of OH^- in dictating the size and shape of Au nanowires is unknown. In this manuscript, we show the first example of the influence of OH^- during the green synthesis of Au NWs in extreme alkaline conditions. It should be noted that the impact of OH^- during the formation of Ag nanowires has been reported earlier; however, in that case, the high concentration of OH^- decreased Ag nanowire formation.[41] To our knowledge, this is the first report that illustrates the selective synthesis of Au NWs in extreme alkaline conditions using a simple one-pot, green synthetic approach by completely eliminating toxic chemicals like $NaBH_4$. The size and shape can be skillfully tuned by just altering the pH environment. The growth mechanism of nanowire formation proposes that elongation occurs in the [110] facet of Au [110], as opposed to the [100] or [111] facets. It is also established that the catalytic activity of such Au NWs is 10-fold more efficient, compared to Au NPs.

Materials and methods

Materials

The chemicals were used directly without further purification and were dissolved in double distilled water. Gold(III) chloride hydrate (99.999% trace metal basis) was obtained from Aldrich. Cetyltrimethylammonium bromide (CTAB) (Acros Organics), and curcumin (Sigma) were used as received. Silver nitrate ($AgNO_3$) and sodium borohydride ($NaBH_4$) were obtained from Sigma Aldrich. 1,2-Dipalmitoyl-*sn-glycero*-3-phosphocholine (DPPC) lipids were obtained from AVANTI products.

Preparation of liposomes

DPPC liposomes were prepared by a solvent evaporation method.[42] The desired amount of DPPC phospholipid was dissolved in 15 mL of a mixture of chloroform–methanol at 2 : 1 volume ratio. The solvents were evaporated using a rotary evaporator at 57 to 60 °C. The membrane formed was dried under vacuum for 10 minutes. Glass beads were added, and enough phosphate buffer at pH 7.0 or double distilled water was used to form liposomes at a concentration of 1 mM. The mixture was vortexed rigorously for 15 minutes and finally heated for 30 minutes at 60 °C, above the phase transition temperatures for DPPC. When required, further dilution was made in double distilled water. The prepared liposomes were multi-lamellar vesicles.

Synthesis of gold nanoparticles/nanowires

The preparation of gold nanoparticles was done as described below using CTAB or DPPC liposomes and with/without silver nitrate. Briefly, 0.27 g of CTAB was dissolved in 15 mL of double distilled water heated at 60 °C (for of DPPC liposomes, 50 μL of liposomes were used instead of CTAB) and the solution was kept for 2 minutes in water at 30 °C. Then, 1 mL of 4 mM $AgNO_3$ was added (in the case without $AgNO_3$, this step was avoided)

and the solution was kept for 15 minutes in water at 30 °C. To the mixture, 1 mL of NaOH at pH 13 (other pH environments were changed accordingly) was added after adding the gold solution prepared in 15 mL double distilled water and stirred for 2 min at 400 rpm. Finally, 0.03 g of curcumin in methanol was added to the solution. The final solution was kept for 1 day at 45 °C. The solution was centrifuged at 1000 rpm for 5 min and at 15 000 rpm for 25 min to precipitate the gold. Four procedures were applied, as outlined below, during synthesis.

Procedure 1: 50 mM CTAB + 1 mM gold + 100 mM of curcumin + 4 mM $AgNO_3$

Procedure 2: 50 mM CTAB + 1 mM gold + 100 mM of curcumin

Procedure 3: 0.03 mM liposome + 1 mM gold + 100 mM of curcumin + 4 mM $AgNO_3$

Procedure 4: 0.03 mM liposome + 1 mM gold + 100 mM of curcumin.

Characterization and spectroscopic analysis

The absorption spectra were recorded at room temperature using a JASCO V-570 UV-VIS-NIR spectrophotometer. The particle size distribution was analyzed using the DLS (Brookhaven Instruments Corps) technique with a laser source of 658 nm and a PMT detector (HAMAMATSU, HC120-30). The software used was 90Plus Particle Sizing Software Ver. 5.23 and the dust was set at 40. The X-Ray Diffraction (XRD) data were collected using a Bruker d8 discover X-ray diffractometer equipped with Cu-Kα radiation (λ = 1.5405 Å). The monochromator used was the Johansson type. Scanning electron microscopy (SEM) analysis was done using Tescan, Vega 3 LMU with Oxford EDX detector (Inca XmaW20). In short, a few drops of gold solution were deposited on an aluminum stub and coated with carbon conductive adhesive tape. FT-IR spectra were recorded on a FT-IR-Raman spectrometer. A Thermo Nicolet 4700 Fourier Transform Infrared spectrometer equipped with a class 1 laser was used for this purpose. The KBr pellet technique was applied to perform the transmission experiments in the range between 3200 and 500 cm^{-1}. The thermogravimetric analysis (TGA) and differential scanning calorimetry (DSC) measurements were done using a Netzsch TGA 209 in the temperature range of 30 to 800 °C with an increment of 10 °C min^{-1} in a N_2 atmosphere. The emission and excitation measurements were documented with resolution increment of 1 nm and slit 5 nm using a Jobin-Yvon-Horiba Fluorolog III fluorometer and the FluorEssence program. The excitation source was a 100 W xenon lamp, and the detector used was R-928, operating at a voltage of 950 V. Synchronous fluorescence scans were obtained using the same instrument by keeping the excitation and emission wavelength interval at 0 nm.

Catalysis study

The catalytic reactions were conducted by mixing 0.15 mM of 4-nitrophenol in aqueous solution with 15 mM of freshly prepared $NaBH_4$ aqueous solution in a 3 mL quartz cuvette. Unless otherwise mentioned, 0.5 mL of gold solution was used as the catalyst. The reduction in the optical absorption peak of 4-nitrophenol was determined from the UV-Vis spectrum by using a UV-Vis spectrophotometer. The kinetics of the reaction was studied by following the optical absorption peak of 4-nitrophenol at ~400 nm.

Results and discussion

The importance of CTAB and $AgNO_3$ during Au nanowire formation

A seedless, green synthetic method was used to prepare gold nanoparticles using four different conditions as described in the Materials and methods section. For the synthesis of Au NPs, CTAB was successfully used as the reaction media. CTAB micelles have also been the most preferred media to prepare gold nanorods using seed solution. In addition, CTAB is extremely helpful in solubilizing hydrophobic curcumin; initially, the reduction of Au salt to Au NPs was carried out by curcumin in CTAB micellar media. Further, to understand the behavior of the reaction media, DPPC liposomes were used instead of CTAB micelles during preparation because liposomes are spherical vesicles with more than one lipid bilayer structure. DPPC liposomes were also found to be as effective as CTAB for solubilizing curcumin in the investigated concentration range.[42] Green synthesis was carried out in double distilled water and the pH was adjusted as desired at 45 °C, as illustrated in Scheme 1. Curcumin absorbs prominently in the UV-visible region[42,43] at around 266 nm ($S_0 \rightarrow S_2$ transition) and at around 426 nm ($S_0 \rightarrow S_1$ transition) in water. However, the surface plasmon resonance (LSPR) absorption of Au NPs appears at >500 nm; thus, the identification of absorption peaks >500 nm makes it easier for establishing the formation of Au NPs in the solution.[20] It should be noted that the LSPR excitation wavelength is strongly dependent on the size of the gold nanoparticles, due to the fact that at the LSPR wavelength gold nanoparticles exhibit an enormous electric field enhancement extending from their surface.[44] Except at alkaline pH, curcumin in CTAB or liposome media gave a yellowish color, whereas Au NPs exhibited a dark purple color, which is related to their intensity and size, owing to the localized LSPR. Thus, a visual color change was used as the indicator of the formation of Au NPs, which was subsequently confirmed by UV-visible spectral measurements.

The UV-Vis spectra of Au NPs obtained for the four different procedures (see Materials and methods section) are given in Fig. 1A. The Au NPs prepared in the presence of $AgNO_3$ in CTAB media (procedure 1) gave a LSPR peak at ~546 nm, whereas in the absence of $AgNO_3$ (procedure 2), the peak was found to be at ~539 nm. On the other hand, the LSPR peak obtained in DPPC liposome media was at ~512 nm and ~542 nm in the presence (procedure 3) and absence (procedure 4) of $AgNO_3$, respectively. Based on elastic scattering phenomena, surface plasmon resonance (SPR) or resonance Rayleigh scattering (RRS) have recently been utilized[45] in nano-chemistry research. SPR is produced when the wavelength of Rayleigh scattering is located at or close to the molecular absorption band. SPR/RRS can be measured by applying synchronous fluorescence spectroscopy (SFS) by keeping the wavelength interval ($\Delta\lambda$) at 0 nm.[45] The SPR spectra of Au NPs obtained for four different

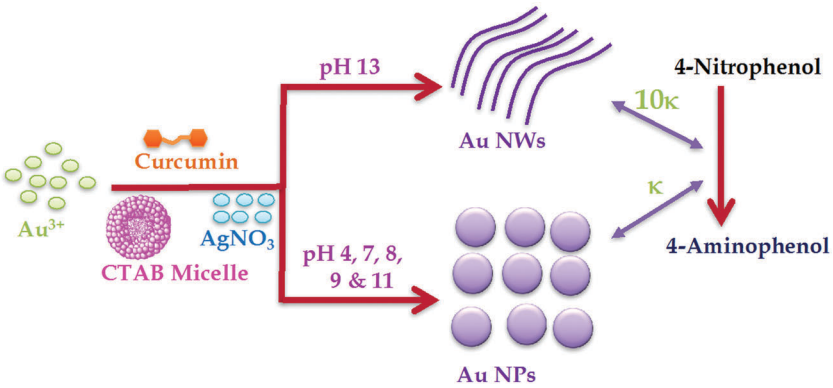

Scheme 1 Illustration of the green synthesis of gold nanowires (Au NWs) and gold nanoparticles (Au NPs) at different pH by reducing Au^{3+} to Au^{0} using curcumin in CTAB media in the presence of $AgNO_3$. The right side of the scheme shows the 10-fold increase in rate constant (κ) for the reduction of 4-nitrophenol to 4-aminophenol in the presence of Au NWs catalysts, compared to Au NPs catalyst.

procedures are shown in Fig. 1B. Au NPs prepared in CTAB media gave two major SPR peaks at ~377 nm and ~548 nm and a minor peak at ~430 nm. However, peaks at ~377 nm and ~430 nm showed a red shift and the peak at ~548 nm gave a blue shift for Au NPs prepared in DPPC liposome media. This could be due to a change in the size of the particles, which was later on confirmed from SEM images depicted in Fig. 2. Interestingly, procedure 1 gave Au nanowires (Au NWs) with a diameter of about 20–25 nm and length >1 μm, whereas procedure 2 gave a particles of diameter 25 to 30 nm (both prepared in CTAB media). Procedures 3 and 4 gave particles of diameter in the range 8 to 15 nm, suggesting that smaller particles are expected in the presence of DPPC liposomes with or without $AgNO_3$. However, no nanowires were obtained in the presence of DPPC liposomes. The shift observed earlier in the UV-visible and SPR spectra also confirmed that different sizes were obtained in CTAB micelles *vs.* DPPC liposomes. The smaller size in liposome media could be due to the protection of Au NPs by a bilayer structure that discourages contact between the Au salt in aqueous solution and the formed Au NPs, which inhibits further growth of the Au particles. Thus, the presence of CTAB micelles and $AgNO_3$ in the solution is crucial for Au nanowire formation during reduction of Au^{3+} by curcumin.

The role of OH^- during Au nanowire formation

Since nanowires obtained using procedure 1 at pH 13 through the present green synthetic route were found to be interesting, the effect of pH was investigated during the synthesis of Au nanowires for procedure 1 only (CTAB micelle and $AgNO_3$). During synthesis, the pH of the medium was varied from 4 to 13 by using acid or alkali. The pH of the medium had a significant influence on the color of the solution. In acidic and moderately alkaline conditions (pH < 11), the obtained nanoparticles were of a dark orange color (similar to the color of curcumin), whereas in extreme alkaline conditions (pH = 13), they turned completely deep red as shown in Fig. 3A. This color change was well reflected in the LSPR peaks. At pH 4, the LSPR peak was found to be at ~572 nm (see Fig. 3B), which shifted to at ~574 nm at pH 7. When the pH of the media was further changed to 8, 9 and 11, the LSPR peak remained at ~572 nm. As discussed earlier, this peak was found to be at ~546 nm at pH 13. A similar result was obtained in SPR spectra shown in Fig. 3C, in which a blue shift of SPR spectra was obtained at pH 13,

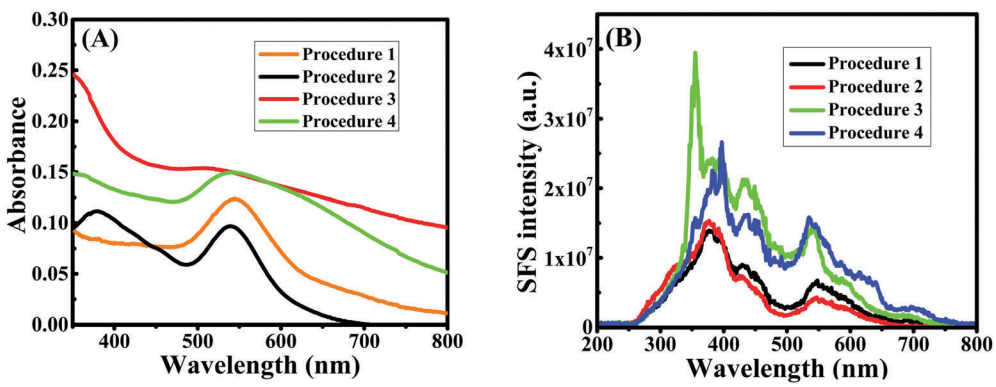

Fig. 1 UV-Vis spectra (A) and synchronous fluorescence spectra at $\Delta\lambda$ = 0 nm (B) of curcumin conjugated Au nanoparticles/nanowires prepared under four different conditions. Procedure 1 is in the presence of curcumin and CTAB with $AgNO_3$; procedure 2 is in the presence of curcumin and CTAB without $AgNO_3$; procedure 3 is in the presence of curcumin and DPPC liposomes with $AgNO_3$; procedure 4 is in the presence of curcumin and DPPC liposomes without $AgNO_3$.

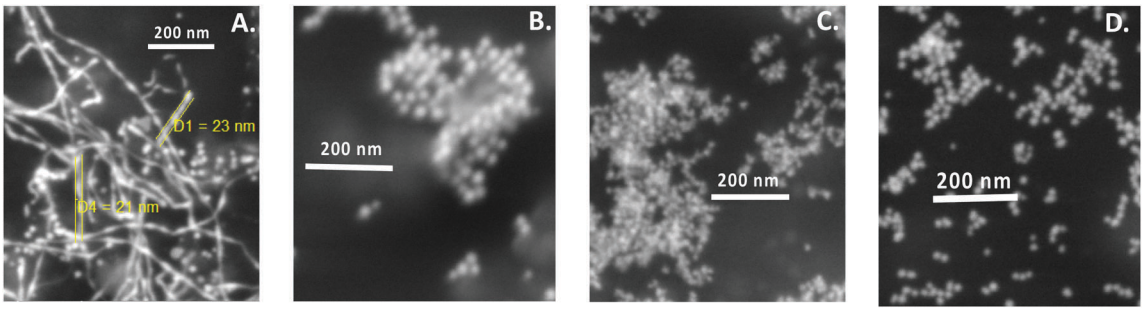

Fig. 2 SEM images of curcumin conjugated gold nanoparticles/nanowires prepared under four different conditions. (A) Procedure 1: in the presence of curcumin and CTAB with $AgNO_3$; (B) procedure 2: in the presence of curcumin and CTAB without $AgNO_3$; (C) procedure 3: in the presence of curcumin and DPPC liposomes with $AgNO_3$; and (D) procedure 4: in the presence of curcumin and DPPC liposomes, without $AgNO_3$.

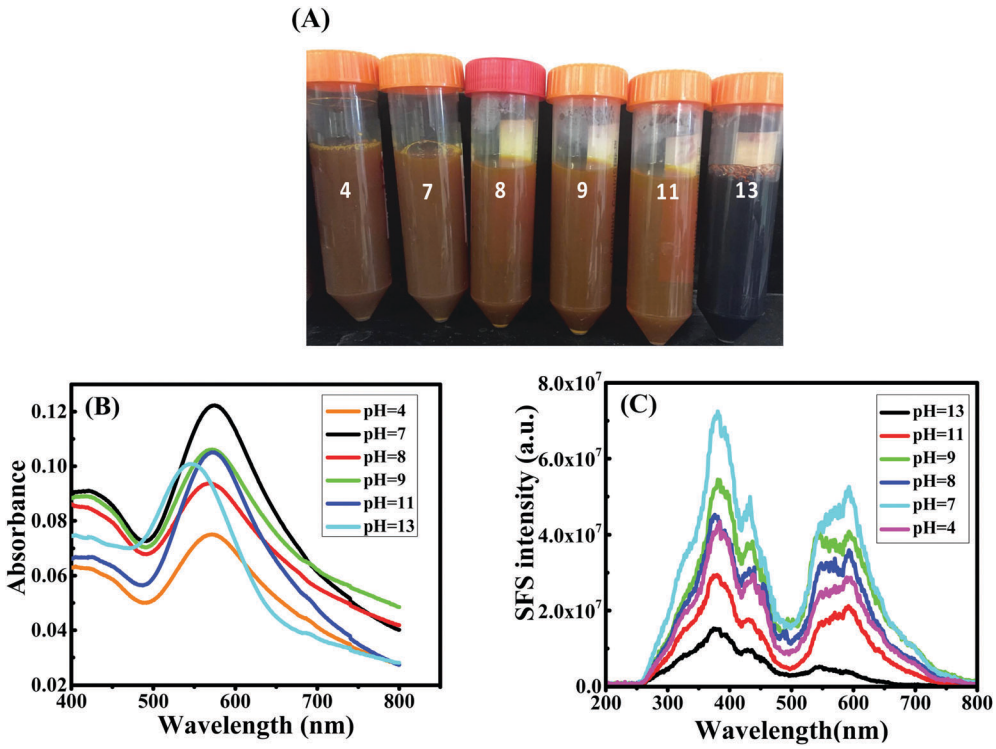

Fig. 3 (A) Photograph of curcumin conjugated gold nanoparticles/nanowires obtained during the green synthesis at different pH values. UV-Vis spectra (B) and synchronous fluorescence spectra at $\Delta\lambda$ = 0 nm (C) of gold nanoparticles/nanowires prepared at different pH values.

compared to pH 4, 7, 8, 9 and 11. SEM images depicted in Fig. 4 confirmed that the particles obtained at pH 4, 7, 8, 9 and 11 were largely spherical in shape with a diameter of about 50–70 nm; however, there were a few cylindrically shaped rods with diameter of about 50–60 nm and length of about 100–120 nm. Nevertheless, at pH 13, nanowires were obtained as discussed earlier, suggesting that the pH of the medium is crucial during the preparation of curcumin conjugated Au nanowires, and an excess of OH^- is needed for the formation of the nanowires.

The role of Ag^+ during Au nanowires/nanoparticles formation

EDX analysis, depicted in Fig. 5, established the presence of Au peaks and carbon peaks as expected, due to capping of CTAB/curcumin, but did not show any peak for Ag under any of the pH conditions, suggesting that $AgNO_3$ only helped in the formation of Au NPs/NWs. This result is similar to our earlier finding during the preparation of Au nanorods using the seed method in the presence of $AgNO_3$.[20] To further establish the characteristics of Au NPs/NWs, the gold nanoparticles and nanowires generated at pH 7 and 13 were analyzed by X-Ray Diffraction (XRD) (see Fig. 6). The X-ray diffractograms were similar for both Au NWs and NPs prepared at two different pHs. The characteristic peaks at 38.269°, 44.600°, 64.678°, 77.549° were assigned to the (111), (200), (220), and (311) reflections of the face centered cubic unit cell, which is typical for Au particles.[21,46] This further proves that the role of Ag^+ is only to facilitate the formation of Au NPs/NWs.

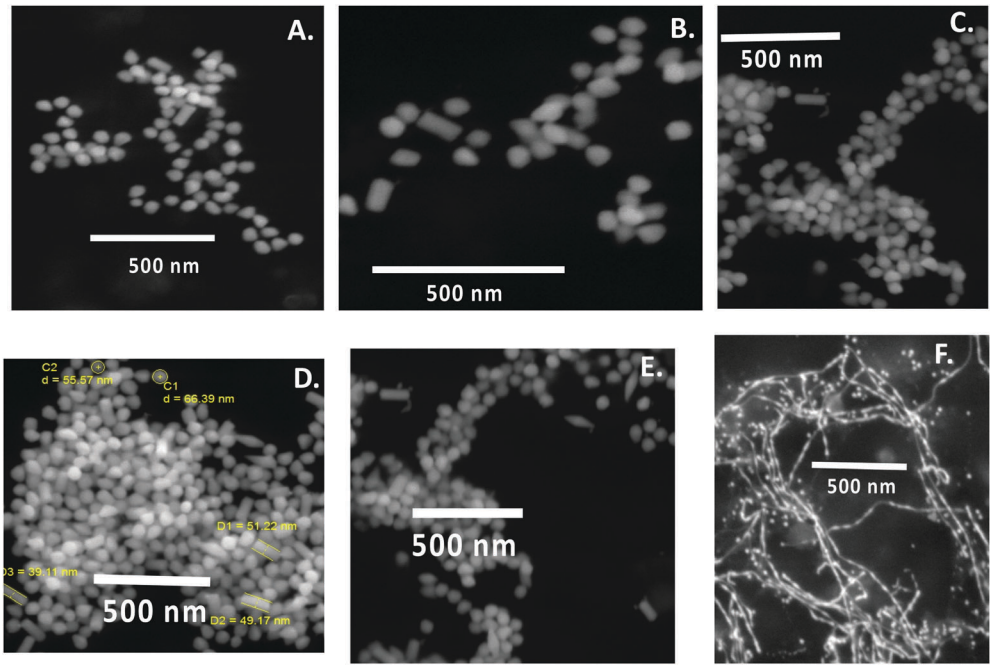

Fig. 4 SEM images of curcumin conjugated gold nanoparticles/nanowires prepared at pH (A) 4; (B) 7; (C) 8; (D) 9; (E) 11 and (F) 13.

The role of curcumin and CTAB during Au nanowires/nanoparticles formation

Thermogravimetric analysis showed the decomposition of CTAB, curcumin and $AgNO_3$ at ~279 °C,[47] ~400 °C[48] and ~470 °C,[49] respectively, as given in Fig. 7A, which is consistent with other reported values. TGA data for the Au NPs (prepared at pH 7) and Au NWs (prepared at pH 13) illustrated similar degradation patterns; both demonstrated a significant weight loss of ~50% at ~300 °C, indicating that both Au NPs, as well as Au NWs were capped with ~50% of CTAB. However, some of these weight losses could also be due to the presence of curcumin. Additionally, a ~10% weight loss for Au NPs/NWs between 300 °C and 400 °C was due to curcumin alone. Interestingly, no loss of water was observed at around 100 °C and it can be assumed that the samples were dehydrated; thus, the nanoparticles/nanowires that were formed are stable.[21] TGA data for both Au NWs (prepared at pH 13) and NPs (prepared at pH 4 to 11) also imply that both these particles were capped with similar percentages of CTAB; this was evident from DLS measurements as well. The effective diameters of Au nanoparticles/nanowires obtained by DLS measurements at pH 4, 7, 8, 9, 11, and 13 were 273 nm, 217 nm, 237 nm, 251 nm, 205 nm and 212 nm, respectively, with their respective polydispersities of 0.27, 0.26, 0.28, 0.29, 0.29 and 0.25. The higher estimated size distribution in DLS measurement, compared to SEM, could be due to the aggregation of the particles in solution. Since Au NWs and NPs have similar percentages of CTAB as found from TGA, they are expected to form similar kinds of aggregations in solution.

Differential scanning calorimetry (DSC) measures the energy absorbed (endothermic) or produced (exothermic) as a function of time or temperature. It is used to characterize melting, crystallization, resin curing, loss of solvents, and other processes involving an energy change. The DSC curves for Au NPs and NWs were compared with those of CTAB and curcumin as shown in Fig. 7B. The DSC curve of CTAB showed a solid–solid transition temperature at ~106 °C, which is the same as the reported value,[47] and is due to the melting temperature of CTAB tails as a result of the transition from the ordered to disordered state.[50] This phase transition temperature of CTAB shifted to 105 °C in Au NWs (prepared at pH 13) and 101 °C in Au NPs (prepared at pH 7), signifying that the alignment of CTAB tails is marginally influenced by the shape of the Au NPs/NWs. Curcumin did not show any phase transition in this temperature range, except an endothermic peak at 178 °C, which is consistent with the literature.[48] The endothermic peaks at 130 °C and 146 °C for Au NPs (prepared at pH 7) and Au NWs (prepared at pH 13), respectively, can be due to the desorption of free and uncomplexed CTAB/curcumin molecules. The endothermic peak at ~270 °C for pure CTAB is attributed to the decomposition of CTAB molecules, thus, the peaks around 230–250 °C for Au NPs and 245–260 °C for Au NWs might be due to the decomposition of CTAB/curcumin molecules from the Au surfaces.

The role of curcumin and CTAB during conjugation/capping of NPs/NWs was further established by spectroscopic analysis. The FT-IR spectra for pure CTAB, Au NPs prepared at pH 7, Au NWs prepared at pH 13 and pure curcumin are exhibited in Fig. 8. In the spectral region 3200–2500 cm^{-1}, the C–H symmetric (stretching) and asymmetric (anti-stretching) vibration frequency modes at 2850 and 2919 cm^{-1}, respectively, were seen for pure CTAB, meaning that it is a crystalline phase, which is distinguished from a micelle conformation. For pure CTAB, less intense peaks were observed at 3014, 1491 and 1453 cm^{-1},

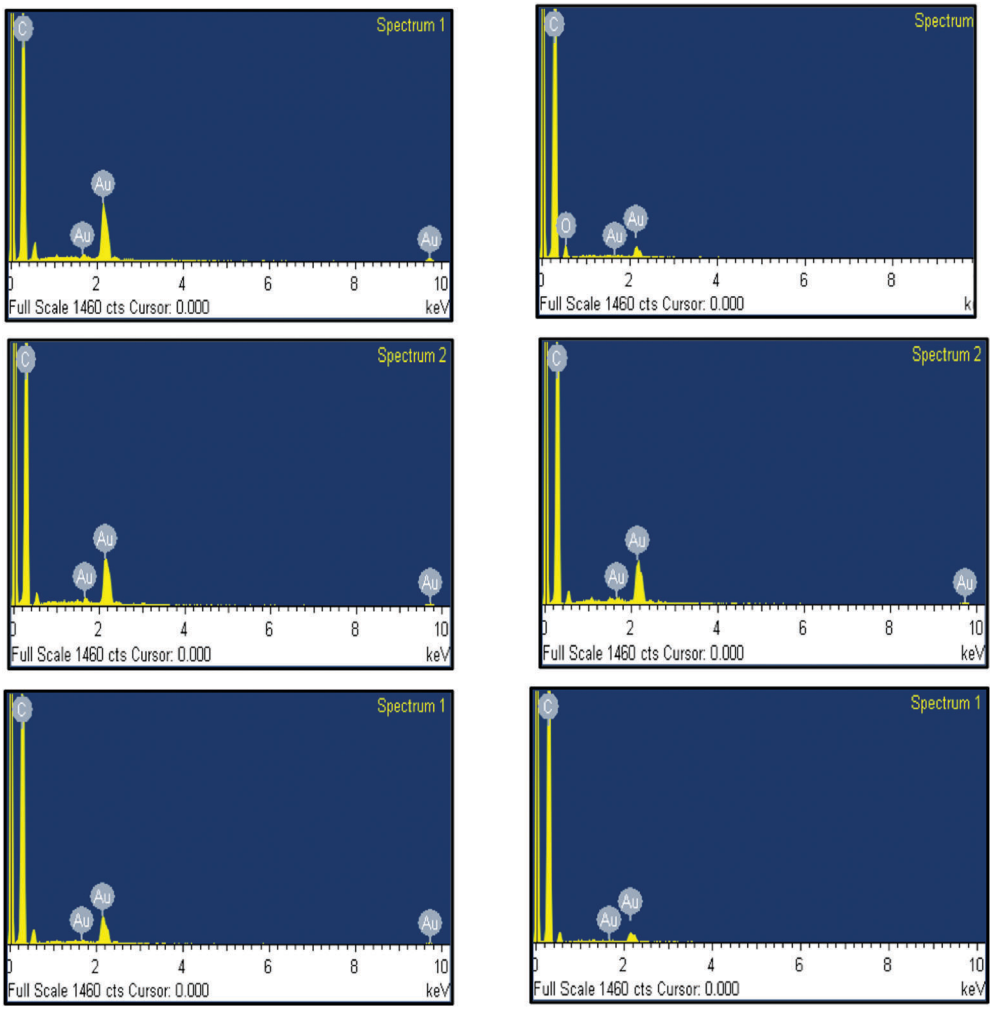

Fig. 5 EDX of curcumin conjugated gold nanoparticles/nanowires prepared at pH 4, 7, 8, 9, 11 and 13, respectively.

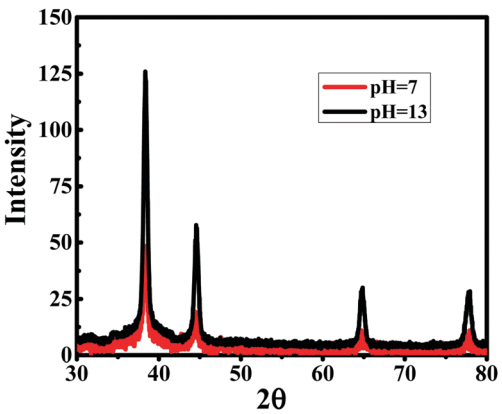

Fig. 6 X-ray diffraction patterns of curcumin conjugated gold nanoparticles and nanowires prepared at pH 7 and 13, respectively.

attributed to the asymmetric and symmetric C–H scissoring vibrations of CH_3–N^+moieties and to the CH_2 scissoring mode. The 1300–1680 cm^{-1} region also signifies the CH_2 scissoring mode of vibration. All these sharp peaks in pure CTAB were also present or slightly shifted, but with low intensity in the case of the gold nanoparticles/nanowires, which indicates an interaction of CTAB and the Au NPs/NWs surface. Concerning the FT-IR spectrum of curcumin, the strong peak at 1630 cm^{-1} has a predominantly mixed ν(C–C) and ν(C═O) character. Another strong band at 1601 cm^{-1} is attributed to the symmetric aromatic ring stretching vibrations ν(C–C_{ring}). The 1519 cm^{-1} peak is assigned to the (C═O). The enol C–O peak was obtained at 1262 cm^{-1}, the C–O–C peak at 1018 cm^{-1}, the benzoate *trans*-CH vibration at 978 cm^{-1} and the *cis* CH vibration of the aromatic ring at 703 cm^{-1}. The bands at 1404 cm^{-1} represent the in-plane bending of the hydroxyl groups of the phenolic group. All three bands (1404, 1262 and 978 cm^{-1}) were completely absent in the FT-IR spectrum of Au NPs/NWs, which suggests the interaction of $HAuCl_4$ at these sites. The bands at 774 cm^{-1} and 1424 cm^{-1}, corresponding to the olefinic in-plane bending vibrations of the heptadiene chain of curcumin, were observed in Au NPs/NWs, demonstrating the presence of the intact curcumin moiety in the Au NPs/NWs. Similarly, the bands at 2926 cm^{-1}, 1471 cm^{-1}, 1045 cm^{-1} and 964 cm^{-1} that appeared in Au NWs are due to vibrations of aliphatic C–H stretches and mixed vibrations of

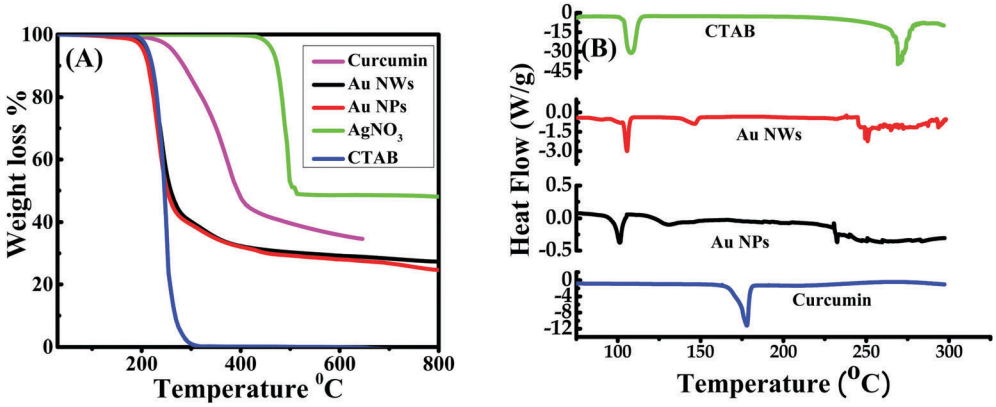

Fig. 7 TGA (A) and DSC curves (B) of CTAB, curcumin and curcumin conjugated gold nanoparticles (Au NPs) and nanowires (Au NWs) prepared at pH 7 and 13, respectively.

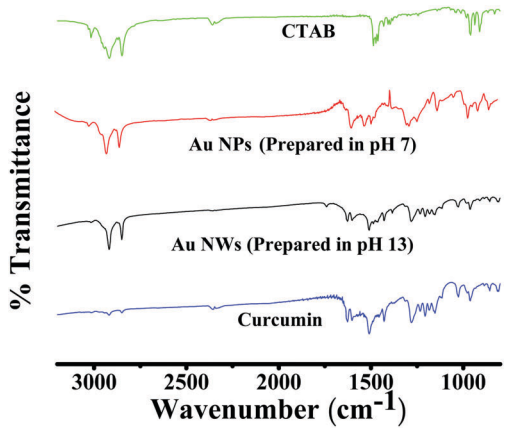

Fig. 8 FT-IR spectra of CTAB, curcumin and curcumin conjugated gold nanoparticles (Au NPs) and nanowires (Au NWs) prepared at pH 7 and 13, respectively.

CH_3, aromatic CCC and CCH of curcumin, confirming the action of curcumin as a capping agent.[9,51,52] The fluorescence emission spectra as presented in Fig. 9 of Au NWs at excitation wavelengths 425 nm and 500 nm gave similar emission with an emission maximum at ~550 nm, which could be due to the presence of curcumin. However, the emission intensity at excitation wavelength 500 nm was found to be remarkably higher than that at excitation wavelength 425 nm. If the emission could be solely due to curcumin, then maximum fluorescence intensity would have come at 425 nm excitation wavelength, which is the absorption wavelength maximum for curcumin. In addition, Au NWs have a strong absorption in the 500 nm range; therefore, the emission reflects that of curcumin conjugated Au NWs, but the contribution from curcumin fluorescence alone cannot be ruled out completely. TGA, DSC, FT-IR and fluorescence analysis clearly advocate the roles of curcumin and CTAB as capping and stabilizing agents; thus, both curcumin and CTAB are immediately accessible to Au^{3+}, which suggests that Au^{3+} is present at the Stern layer of CTAB micelles during reduction to form either Au NWs or NPs, depending on the pH of the medium.

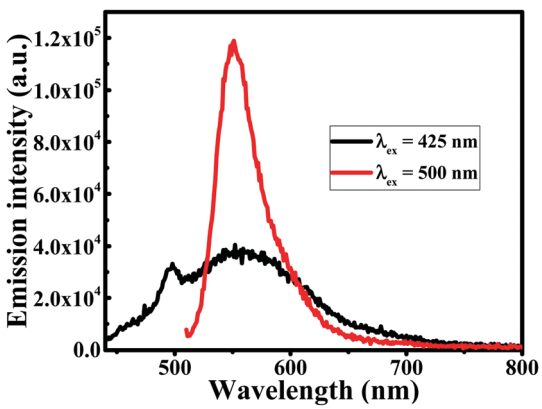

Fig. 9 Fluorescence emission spectra of gold nanowires (Au NWs) prepared at pH 13, at excitation wavelengths (λ_{ex}) 425 nm and 500 nm.

Kinetics and growth mechanism of Au nanowire formation

The kinetics of the reaction to form Au NWs was followed in two different ways. First, the depletion of the curcumin concentration was monitored by measuring the change in absorbance of curcumin in the reaction mixture (before centrifugation) at 425 nm. The absorbance of curcumin decreased with the production of Au NWs and was saturated after 20 h; the rate of reduction in curcumin absorbance with time is plotted in Fig. 10A. The rate constant for the depletion of curcumin concentration was estimated as 0.13 h^{-1}. Secondly, to understand the growth mechanism, the morphology from the initial particle formation to nanowire formation was examined. In this case, the kinetic of formation of Au NWs was followed by stopping the reaction in a given time interval and separating the Au NPs/NWs after centrifugation. During the growth of both Au NWs and NPs, initially the LSPR peak in the UV-visible spectrum was found at ~512 nm, which could be due to the formation of smaller nanoparticles. After 1 h and 2 h, the shift in the LSPR peak was marginal (~515 nm), which subsequently shifted to ~546 nm for Au NWs and ~574 nm for Au NPs after 24 h. The absorbance of the collected Au NPs/NWs was monitored as shown in Fig. 10B and it was found that the

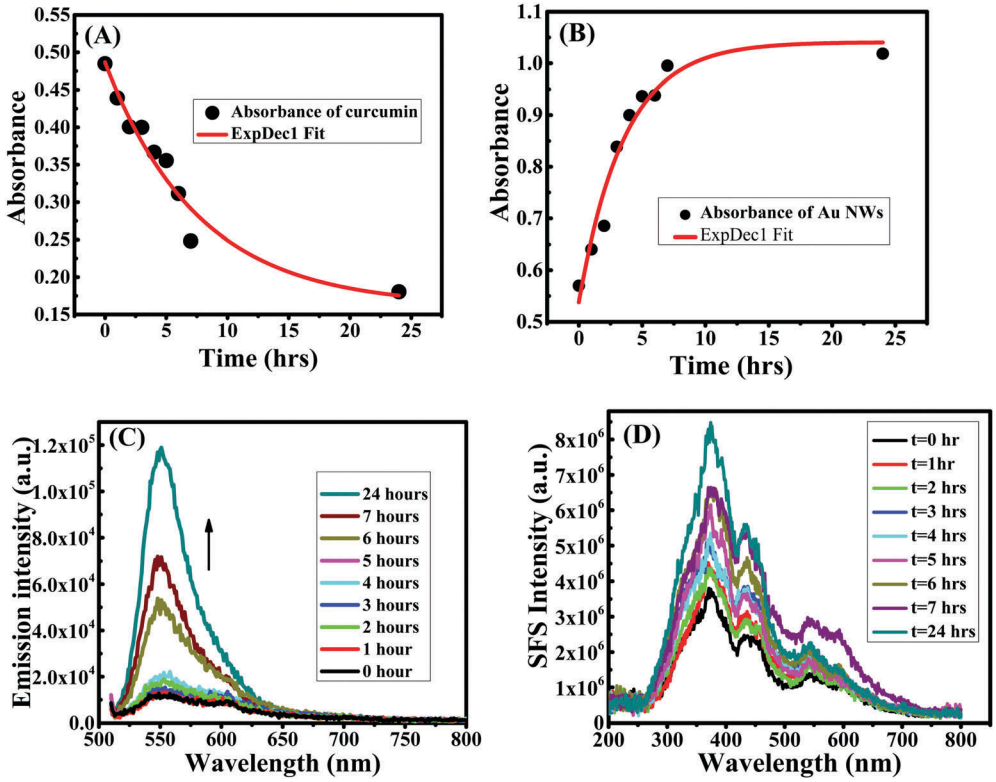

Fig. 10 Changes in absorbance of curcumin (A) and Au NWs (B) during synthesis under extreme alkaline conditions. Fluorescence emission spectra (C) and synchronous fluorescence spectra at $\Delta\lambda$ = 0 nm (D) during the preparation of curcumin conjugated gold nanowires (Au NWs) at pH 13 and for different times.

absorbance increased continuously for 5 h and then afterwards it became saturated. The increase in absorbance is due to the formation of more Au NP/NWs. The estimated rate constant for the formation of Au NWs in this case was $\sim$0.28 h^{-1}. The difference in the rate of depletion of curcumin and rate of formation of Au NWs is marginal and comparable; however, this marginal difference in rate constant could be attributed to the degradation of curcumin during the reaction time, which is not surprising as the degradation of curcumin in alkaline medium is well reported.[53] Interestingly, the fluorescence intensity of Au NWs increased with time as the reaction proceeded, as shown in Fig. 10C, which is evidence of an increase in curcumin content with the growth of NWs; thus, the growth of Au nanowires is accompanied by curcumin capping/conjugation. The intensity in the SPR spectra (see Fig. 10D) was enhanced with time during nanowire formation, which is obvious since both the particle size and mass of nanoparticles increased with the growth of the nanowires. The morphology of growth of Au NWs was also followed by SEM, as shown in Fig. 11. Within a few minutes ($\sim$10 minutes), one could be able to see the formation of small Au NPs with a few small nanorod/nanowire structures, but no larger nanowires were detected in the beginning. However, after 1 h, there was nanowire growth and/or connections started appearing between nanoparticles without a remarkable change in the thickness of the particles. The aggregation of the particles was more visible with time and after 24 h, the shapes of the nanowires were clearly visible.

Based on the above pH study and kinetic data, the following rationale could be made. Curcumin is closely available to $AuCl_4^-$ ions at the micelle surface because of its hydrophobic nature, which facilitates the reduction of $AuCl_4^-$ to $AuCl_2^-$ at the micelle surface. These formed nanoparticles are stabilized by the immediately available CTA^+ at the micellar surface, as evident from TGA, DSC and spectroscopic data. During the start of the reaction, smaller Au NPs are formed in all pH environments. As the reaction proceeds, the particles grow to different shapes and sizes, depending on the pH environment. As discussed earlier, at pH 4 to 11, relatively large sized spherical gold nanoparticles, along with a few non-spherical structures such as cylindrical rods were observed. This is similar to our earlier findings[20] during the synthesis of gold nanorods using seed solution, where all seeds grew isotropically until a critical size for transition was reached.[54] This happened as the particles grew isotropically in all directions, due to clusters with the [111] facets of Au.[54] The poor yield of nanorods in the presence of $AgNO_3$ is also consistent with our earlier finding, where none or very few nanorods were found for CTAB capped Au NPs seed solution in the presence of $AgNO_3$ using curcumin.[20] Since the Au NPs formed were capped with CTAB and were typically spherical particles (see Fig. 4), the growth of NPs had to occur at the micellar interface. Based on the mechanism proposed by Nikoobakht and El-Sayed,[2] silver ions are located between the head groups of CTAB as Ag–Br pairs (see Scheme 2, left), thus, curcumin and the silver ions can come close to each other at the

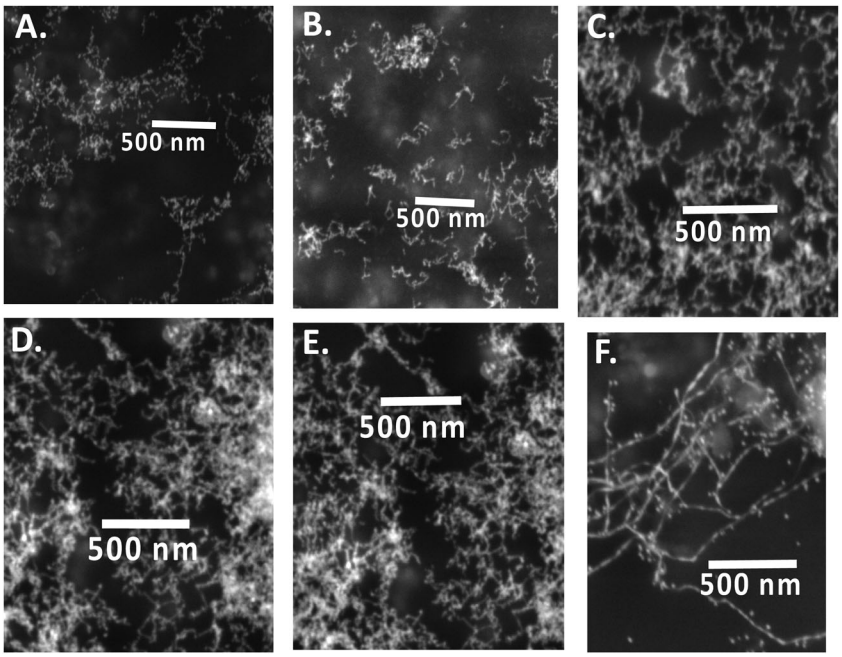

Fig. 11 SEM images of curcumin conjugated gold nanowires prepared at pH 13 at different times: (A) 10 minutes, (B) 1 h, (C) 2 h, (D) 4 h, (E) 7 h and (F) 24 h.

Stern layer of the micelle, although hydrophobic interactions between the alkyl chain of the CTAB molecule and curcumin at pH <11 makes curcumin orient itself parallel to the hydrophobic chain of CTAB, as shown in Scheme 2, left. In this case, the Ag monolayer will occupy the facet of Au and subsequently, Ag will be oxidized and replaced by Au to form relative larger Au NPs. Nevertheless, it must be noted that the presence of Ag^{+} only accelerates the process, as Au nanoparticles can still be formed by directly reducing Au^{3+} by curcumin in the absence of Ag^{+} ions.

The situation is not the same at pH 13. Curcumin is completely deprotonated and more water soluble at this pH, which drives curcumin to be present in the Stern layer of the CTAB micelle (by orienting itself perpendicular to the hydrophobic chain of CTAB as shown in Scheme 2, right) instead of buried inside the hydrophobic pocket; however, this further encourages more contact between curcumin and the Ag^{+} ion. In Au NPs, the surface energy of the [110] facets is higher than that of the [100] facets and [111] facets; thus, the [110] facets must be unstable and exposed.[55] From the mechanism proposed by Guyot-Sionnest and coworkers, the potential deposition of silver occurs preferentially on the [110] gold facets, compared to the [111] and [100] facets, leading to anisotropic growth in the [110] direction.[56] Since the Ag monolayer will occupy the [110] facet of Au as illustrated in Scheme 2 (right), other facets [100] and [111] will not grow as expected, compared to the [110] facet. Moreover, curcumin is chemically a β-diketone that tautomerizes between its enol and keto structures. Theoretical and experimental studies have determined three acidity constants for

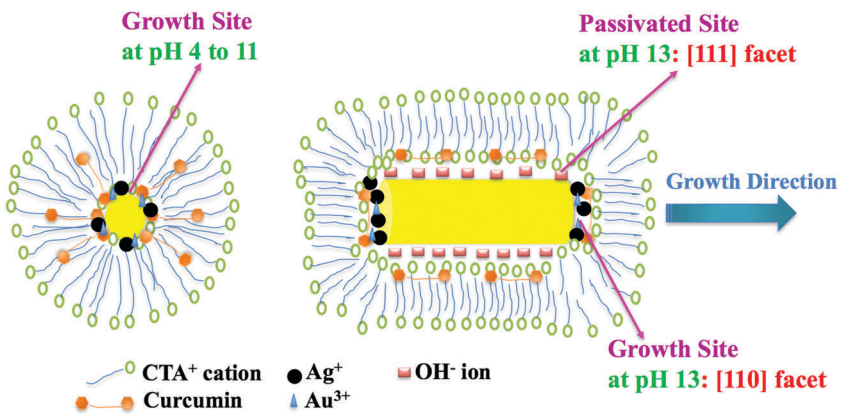

Scheme 2 Illustration (not to scale) of the growth mechanism of gold nanoparticles (Au NPs) at pH 4 to 11 (left) and gold nanowires (Au NWs) at pH 13 (right), by reducing Au^{3+} to Au^{0} using curcumin in CTAB media in the presence of Ag^{+}. The cartoon on the right describes the side growth in the [111] and [100] directions, which is passivated by OH^{-} ions; thus, elongation along the [110] direction is facilitated to form Au nanowires.

curcumin with pK_a values of 7.75, 8.55 and 9.05 from the ionization of enolic and the two phenolic OH protons, respectively.[57] Since the sizes and shapes of the Au NPs obtained in pH 4, 7, 8, 9 and 11 were similar, deprotonation of curcumin may not be the deciding factor for obtained results under extreme alkaline conditions. Earlier, it was reported that OH^- is key to the formation of Ag nanowires,[41] although in this case, the high concentration of OH^- decreased Ag nanowire formation.[41] It is also known that Br-plays a crucial role in the etching interaction with Au NPs; we suspect a similar role at very high concertations of OH^-. Since the etching process occurs much easier in smaller particles than large particles, and the obtained nanowires were unexpectedly thinner (unlike the few nanorods seen in pH 4 to 11), the influence of OH^- cannot be ruled out. We propose that the side facets, [100] and [111], are passivated by OH^- ions and the absence of Ag^+ ions, hence, the side growth is retarded and elongation along the [110] direction is facilitated by the presence of Ag^+ ions (see Scheme 2, right). As per the theoretical calculations by Barnard and Curtiss,[58] the preferred growth of [110] as opposed to [100] or [111] nanorods is energetically favorable. It is assumed that CTA^+ mainly gives steric protection to the formed nanowires. On the other hand, Murphy *et al.* has proposed a different mechanism that falls in line with the above stated one, as it suggests that CTAB would bind preferentially to the Au[100] and [110] facets and then the thermodynamically favorable intermolecular interactions of the 16-carbon cetyl chains take action to promote surface adhesion. This preferential binding regime agrees with the size of the quaternary ammonium head group relative to the larger binding sites available on the Au [100] and Au [110] faces of the crystalline rods, compared to the [111] face.[35,59] In our case, this scenario is also possible, since in the absence of CTAB (or in DPPC liposomes media) no nanowires were detected and we earlier confirmed the conjugation of CTAB on Au surfaces by FT-IR analysis.

Catalytic activity of Au nanowires *vs.* nanoparticles

Catalytic activities of prepared NPs and NWs were tested for nitro-reduction, where 4-nitrophenol was chosen as a model substrate. To investigate the catalytic reduction of 4-nitrophenol using $NaBH_4$, 0.5 mL of Au nanocatalyst was added to 15 mM of freshly prepared $NaBH_4$ and then they were mixed with 0.15 mM of 4-nitrophenol. The total volume was equal to 3 mL. The initial color was yellow, which became transparent after the reduction of 4-nitrophenol to 4-aminophenol. After adding the $NaBH_4$, 4-nitrophenol was reduced to 4-nitrophenolate. The reduction reaction is given below:

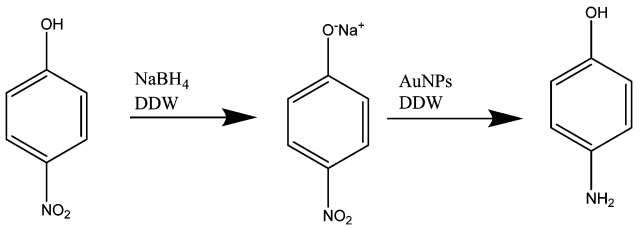

The reduction of 4-nitrophenol was monitored by following the change in the absorbance of 4-nitrophenol at ~400 nm. To ensure the role of the Au NWs/NPs catalysts, two control experiments were performed. Firstly, in the absence of either Au NWs/NPs or $NaBH_4$ the reaction did not progress, as observed from no change in absorbance of 4-nitrophenol with time. Secondly, for the study of the catalyst reduction of 4-nitrophenol, the reduction process was conducted in the absence of Au nanocatalyst. In this case, the relative absorbance of 4-nitrophenolate at ~400 nm decreased significantly with time and a complete reduction of 4-nitrophenol without Au nanoparticles needed approximatively 300 hours (Fig. 12A). The reduction of 4-nitrophenolate to 4-aminophenol was also confirmed the moment a peak at ~290 nm appeared for 4-aminophenol. Therefore, once the total amount of gold present in the solution reacts with the sodium borohydride, 4-aminophenol will be formed.[38,40,60,61] However, in the presence of Au nanocatalyst, the complete reduction of 4-nitrophenolate to 4-aminophenol by $NaBH_4$ was observed within a few minutes, ~4 minutes maximum, (Fig. 12B) revealing that the resultant Au nanocatalyst indeed possessed excellent catalytic activity for the reduction of 4-nitrophenol. It should be noted that the reaction pH should be kept alkaline to ensure the formation of 4-nitrophenolate ions, with plasmon absorption band at 400 nm (pK_a = ~7.15 at room temperature), thus, it is not desirable to investigate the effect of the pH of the reduction reaction of 4-nitrophenol[62] using NWs/NPs as catalyst. Different sizes and shapes of Au NPs/NWs were obtained in the different pH environments used during the preparation of Au NPs/NWs; therefore, the catalytic activities were compared for both NPs and NWs prepared in different pH environments. Even though NPs/NWs prepared at pH 4 to 13 served as excellent catalysts for the reduction of 4-nitrophenol, in all cases, the reaction was completed in a maximum of ~4 minutes, but Au NWs prepared at pH 13 superseded them all.

The estimated rate constant (κ) for the reduction of 4-nitrophenol in the presence of Au NPs/NWs prepared at different pH is presented in Fig. 12C. It was found that the rate constant for nitro-reduction was almost similar for NPs prepared at pH 4, 7, 8, and 9, and it marginally increased for NPs prepared at pH 11. However, for Au NWs prepared at pH 13, the rate constant was remarkably enhanced by ~10 fold, during the reduction of 4-nitrophenol (see Scheme 1, right). This enhancement must be due to the shape and size of NWs compared to NPs. In addition to the anisotropic shape that gives different facets of binding, nanowires are reported to have higher surface areas[63] and surface roughness,[64] which increase the number of active sites to bind to substrates. This explains the significant enhancement in reaction rate during the reduction reaction in the present case. The influence of the concentration of NWs during the catalysis process was tested as shown in Fig. 12D. In the beginning, the reduction rate slightly improved when the concentration of Au NWs was increased from 0.2 mL to 0.5 mL; however, a further increase in NWs concentration to 1 mL and 2 mL did not have any remarkably influence on the reduction rate of 4-nitrophenol.

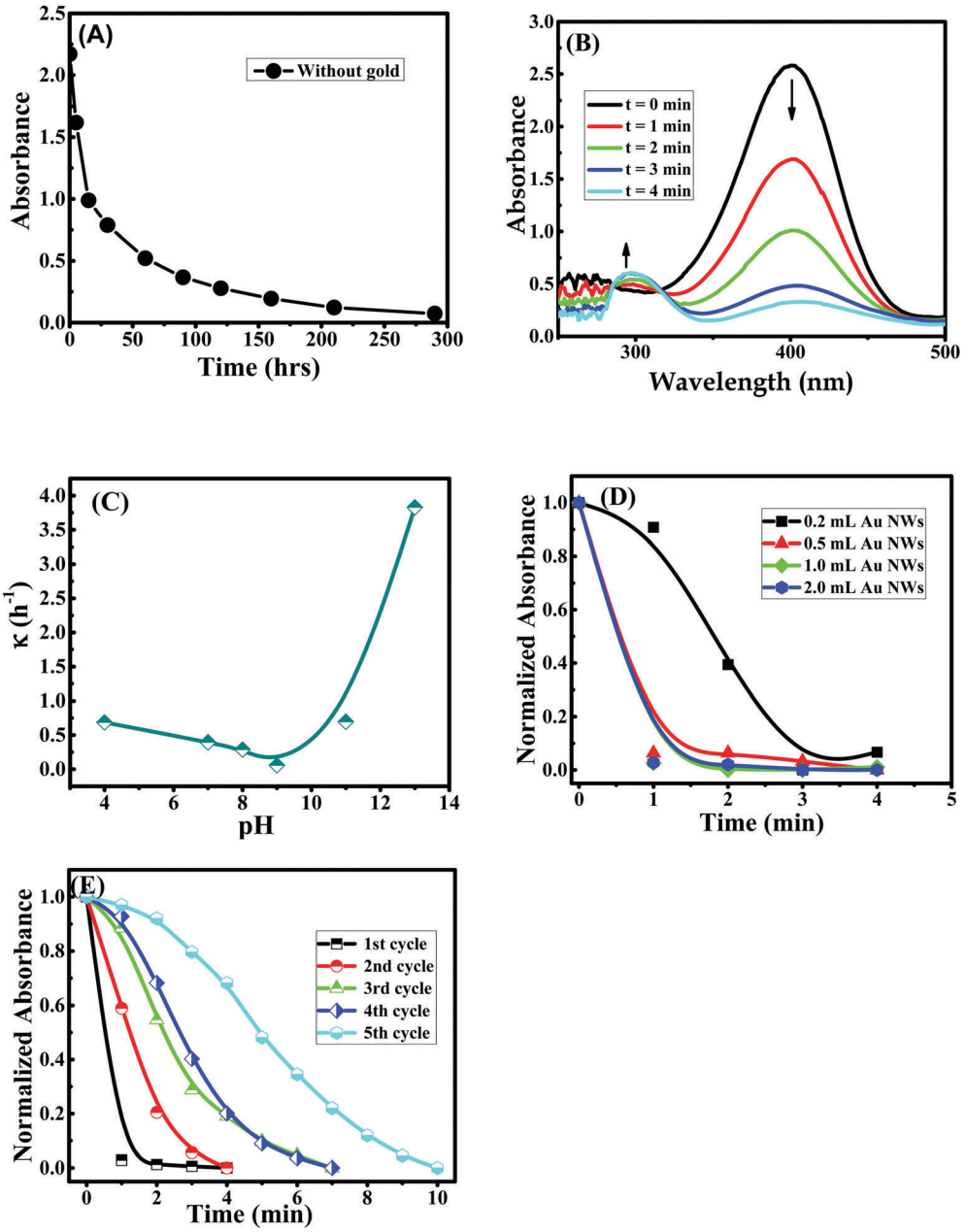

Fig. 12 (A) Change in absorbance of 4-nitrophenol at ~400 nm in the presence of $NaBH_4$ without Au NPs/NWs; (B) UV-visible absorption spectra of 4-nitrophenol in the presence of $NaBH_4$ and Au NPs prepared at pH 7 at different times; (C) variation of rate constant (κ) during the transformation of 4-nitrophenol to 4-aminophenol for Au NPs and NWs prepared at different pH; (D) change in absorbance of 4-nitrophenol at ~400 nm in the presence of $NaBH_4$ and different amounts of Au NWs; (E) change in absorbance of 4-nitrophenol at ~400 nm in the presence of $NaBH_4$ and Au NWs for different reuse cycles.

The recyclability of the catalyst was verified by the following procedure. The catalysts in the reaction cycle were separated after use by centrifugation and reused for the nitro-reduction reaction. As presented in Fig. 12E, the effectiveness of the Au NWs catalyst was present even after the 5th cycle, although there was a slight decrease in the rate constant, which could be due to the loss of the mass during centrifugation. However, using gold nanowires after recycling remained helpful in terms of the reduction of chemical products used and time.

Conclusion

Curcumin capped gold nanowires were successfully prepared *via* a one pot, green synthetic route without using a seed mediated procedure. Au^{3+} ions were reduced to Au^0 by curcumin in CTAB micelles, as well as in DPPC liposome media at pH ranging from 4 to 13, in the presence and absence of $AgNO_3$. Interestingly, this reduction by curcumin in CTAB micelles under extreme alkaline conditions (pH ~13) in the presence of Ag^+ ions preferentially produced Au NWs of diameter ~20–25 nm and

length >1 μm, whereas in the absence of Ag^+, as well as in acidic (pH $\sim$4), neutral (pH $\sim$7) and moderate alkaline conditions (pH $\sim$8, $\sim$9 and $\sim$11), Au NPs of diameter 50–70 nm were obtained instead of Au NWs, which all lead to the conclusion that an excess of OH^- is needed for Au NWs production. However, in both Au NPs and NWs, CTAB and curcumin act as capping and stabilizing agents with no major alteration in their curcumin/CTAB content. The NWs and NPs were found to be stable and crystalline. The use of DPPC liposomes instead of CTAB micelles discouraged the growth of large NPs or NWs generating smaller NPs of diameter $\sim$25 to 30 nm, indicating that the role of CTAB is needed for nanowire formation. The present study suggests that a high concentration of OH^- ions along with the deprotonated form of curcumin and Ag^+ are vital for the preferential formation of Au NWs at pH $\sim$13. The rate of NWs formation was estimated as 0.13 h^{-1}. The results indicate that the growth of NWs happens in the [110] facet of Au [110], as opposed to [100] or [111] facets. The advantage of Au NWs over NPs produced in other pH environments is that curcumin capped Au nanowires were found to be excellent nano-catalysts for the reduction of nitro-compounds. The rate of reduction of 4-nitrophenol by curcumin capped Au NWs was $\sim$10 fold higher than Au NPs prepared in acidic, neutral and moderate alkaline conditions; thus, the present study opens up further study to modify catalytic activities by selectively dictating the size and shape of Au NPs.

Acknowledgements

Financial support provided by National Council of Scientific Research – Lebanon (CNRS-L) and American University of Beirut, Lebanon through URB, Kamal A. Shair Research Fund as well as Kamal A. Shair Central Research Science Laboratory (KAS CRSL) facilities to carry out this work is greatly acknowledged.

References

1 Y. Ying, S.-S. Chang, C.-L. Lee and C. R. C. Wang, *J. Phys. Chem. B*, 1997, **101**, 6661–6664.
2 B. Nikoobakht and M. A. El-Sayed, *Chem. Mater.*, 2003, **15**, 1957–1962.
3 A. P. Alivisatos, *J. Phys. Chem.*, 1996, **100**, 13226–13239.
4 M. A. El-Sayed, *Acc. Chem. Res.*, 2001, **34**, 257–264.
5 G. Schmid, *Chem. Rev.*, 1992, **92**, 1709–1727.
6 A. Eychmüller, *J. Phys. Chem. B*, 2000, **104**, 6514–6528.
7 V. F. Puntes, K. M. Krishnan and A. P. Alivisatos, *Science*, 2001, **291**, 2115–2117.
8 M.-C. Daniel and D. Astruc, *Chem. Rev.*, 2004, **104**, 293–346.
9 K. Sindhu, A. Rajaram, K. J. Sreeram and R. Rajaram, *RSC Adv.*, 2014, **4**, 1808–1818.
10 G. Schmid, *Chem. Soc. Rev.*, 2008, **37**, 1909–1930.
11 E. C. Dreaden, A. M. Alkilany, X. Huang, C. J. Murphy and M. A. El-Sayed, *Chem. Soc. Rev.*, 2012, **41**, 2740–2779.
12 P. M. Tiwari, K. Vig, V. A. Dennis and S. R. Singh, *Nanomaterials*, 2011, **1**, 31–63.
13 J. Kimling, M. Maier, B. Okenve, V. Kotaidis, H. Ballot and A. Plech, *J. Phys. Chem. B*, 2006, **110**, 15700–15707.
14 F. Kim, J. H. Song and P. Yang, *J. Am. Chem. Soc.*, 2002, **124**, 14316–14317.
15 D. K. Smith and B. A. Korgel, *Langmuir*, 2008, **24**, 644–649.
16 B. D. Busbee, S. O. Obare and C. J. Murphy, *Adv. Mater.*, 2003, **15**, 414–416.
17 J.-U. Kim, S. H. Cha, H. Shin, J. Y. Jho and J.-C. Lee, *Adv. Mater.*, 2004, **16**, 459–464.
18 A. Halder and N. Ravishankar, *Adv. Mater.*, 2007, **19**, 1854–1858.
19 M. Grzelczak, J. Pérez-Juste, P. Mulvaney and L. M. Liz-Marzán, *Chem. Soc. Rev.*, 2008, **37**, 1783–1791.
20 R. N. Moussawi and D. Patra, *J. Phys. Chem. C*, 2015, **119**, 19458–19468.
21 A. L. González-mendoza and L. I. Cabrera-Lara, *J. Mex. Chem. Soc.*, 2015, **59**, 119–129.
22 Q. Xu, J. Bao, F. Capasso and G. M. Whitesides, *Angew. Chem., Int. Ed.*, 2006, **45**, 3631–3635.
23 C. A. Foss Jr., M. J. Tierney and C. R. Martin, *J. Phys. Chem.*, 1992, **96**, 9001–9007.
24 J. Polte, T. T. Ahner, F. Delissen, S. Sokolov, F. Emmerling, A. F. Thünemann and R. Kraehnert, *J. Am. Chem. Soc.*, 2010, **132**, 1296–1301.
25 D. Kumar, B. J. Meenan, J. Mutreja, R. D'Sa and D. Dixon, *Int. J. Nanosci.*, 2012, **11**, 1250023.
26 J. Turkevich, *Gold Bull.*, 1985, **18**, 86–91.
27 M. M. Poojary, P. Passamonti and A. V. Adhikari, *J. Bionanosci.*, 2016, **6**, 110–120.
28 V. Kumar and S. K. Yadav, *J. Chem. Technol. Biotechnol.*, 2009, **84**, 151–157.
29 S. P. Chandran, M. Chaudhary, R. Pasricha, A. Ahmad and M. Sastry, *Biotechnol. Prog.*, 2006, **22**, 577–583.
30 D. MubarakAli, N. Thajuddin, K. Jeganathan and M. Gunasekaran, *Colloids Surf., B*, 2011, **85**, 360–365.
31 H. Hatcher, R. Planalp, J. Cho, F. M. Torti and S. V. Torti, *Cell. Mol. Life Sci.*, 2008, **65**, 1631–1652.
32 P. Anand, A. B. Kunnumakkara, R. A. Newman and B. B. Aggarwal, *Mol. Pharmaceutics*, 2007, **4**, 807–818.
33 R. Gangwar, V. A. Dhumale, D. Kumari, U. T. Nakate, S. W. Gosavi, R. B. Sharma, S. N. Kale and S. Datar, *Mater. Sci. Eng., C*, 2012, **32**, 2659–2663.
34 S. Manju and K. Sreenivasan, *J. Colloid Interface Sci.*, 2012, **368**, 144–151.
35 C. J. Johnson, E. Dujardin, S. Davis, C. J. Murphy and S. Mann, *J. Mater. Chem.*, 2002, **12**, 1765–1770.
36 C.-C. Chang, C.-P. Chen, C.-H. Lee, C.-Y. Chen and C.-W. Lin, *Chem. Commun.*, 2014, **50**, 14443–14446.
37 M. Li and G. Chen, *Nanoscale*, 2013, **5**, 11919–11927.
38 J. Das, M. A. Aziz and H. Yang, *J. Am. Chem. Soc.*, 2006, **128**, 16022–16023.
39 J. Tang, D. Tang, J. Huang, B. Qiu and G. Chen, *Biosens. Bioelectron.*, 2011, **26**, 3219–3226.
40 X. Wang, J. Pauli, R. Niessner, U. Resch-Genger and D. Knopp, *Analyst*, 2015, **140**, 7305–7312.

41 K. K. Caswell, C. M. Bender and C. J. Murphy, *Nano Lett.*, 2003, **3**, 667–669.
42 D. Patra, D. Ahmadieh and R. Aridi, *Colloids Surf., B*, 2013, **110**, 296–304.
43 M. Mouslmani and D. Patra, *RSC Adv.*, 2014, **4**, 8317–8320.
44 W. S. Hwang, P. L. Truong and S. J. Sim, *Anal. Biochem.*, 2012, **421**, 213–218.
45 E. El Khoury, M. Abiad, Z. G. Kassaify and D. Patra, *Colloids Surf., B*, 2015, **127**, 274–280.
46 J. Li, H. Feng, J. Li, Y. Feng, Y. Zhang, J. Jiang and D. Qian, *Electrochim. Acta*, 2015, **167**, 226–236.
47 A. Swami, A. Kumar and M. Sastry, *Langmuir*, 2003, **19**, 1168–1172.
48 V. A. Marcolino, G. M. Zanin, L. R. Durrant, M. D. T. Benassi and G. Matioli, *J. Agric. Food Chem.*, 2011, **59**, 3348–3357.
49 J. Liu, J. Liu, S. Song, F. Wang and Y. Song, *J. Mater. Chem. A*, 2014, **2**, 17477–17488.
50 T. Zhang, G. Xu, J. Puckette and F. D. Blum, *J. Phys. Chem. C*, 2012, **116**, 11626–11634.
51 R. B. Viana, A. B. F. da Silva and A. S. Pimentel, *Adv. Phys. Chem.*, 2012, **2012**, 903272.
52 S. R. Ede, U. Nithiyanantham and S. Kundu, *Phys. Chem. Chem. Phys.*, 2014, **16**, 22723–22734.
53 E. D. El Khoury and D. Patra, *J. Phys. Chem. B*, 2013, **117**, 9699–9708.
54 K. Park, L. F. Drummy, R. C. Wadams, H. Koerner, D. Nepal, L. Fabris and R. A. Vaia, *Chem. Mater.*, 2013, **25**, 555–563.
55 C. J. Murphy, L. B. Thompson, D. J. Chernak, J. A. Yang, S. T. Sivapalan, S. P. Boulos, J. Huang, A. M. Alkilany and P. N. Sisco, *Curr. Opin. Colloid Interface Sci.*, 2011, **16**, 128–134.
56 L. Mingzhao and P. Guyot-Sionnest, *J. Phys. Chem. B*, 2005, **109**, 22192–22200.
57 M. A. Tomren, M. Másson, T. Loftsson and H. H. Tønnesen, *Int. J. Pharm.*, 2007, **338**, 27–34.
58 A. S. Barnard and L. A. Curtiss, *J. Mater. Chem.*, 2007, **17**, 3315–3323.
59 C. J. Murphy, T. K. Sau, A. M. Gole, C. J. Orendorff, J. Gao, L. Gou, S. E. Hunyadi and T. Li, *J. Phys. Chem. B*, 2005, **109**, 13857–13870.
60 S. Saha, A. Pal, S. Kundu, S. Basu and T. Pal, *Langmuir*, 2010, **26**, 2885–2893.
61 Y.-C. Chang and D.-H. Chen, *J. Hazard. Mater.*, 2009, **165**, 664–669.
62 M. Li and G. Chen, *Nanoscale*, 2013, **5**, 11919–11927.
63 M. Law, L. E. Greene, J. C. Johnson, R. Saykally and P. Yang, *Nat. Mater.*, 2005, **4**, 455–459.
64 M. Li, Z. Zhao, T. Cheng, A. Fortunelli, C.-Y. Chen, R. Yu, Q. Zhang, L. Gu, B. Merinov, Z. Lin, E. Zhu, T. Yu, Q. Jia, J. Guo, L. Zhang, W. A. Goddard III, Y. Huang and X. Duan, *Science*, 2016, **354**, 1414–1419.